Modeling of the Pulsed Inductive Thruster, (PIT) operating with Ammonia Propellant

IEPC-2005-128

Presented at the 29th International Electric Propulsion Conference, Princeton University, October 31 – November 4, 2005

Pavlos G. Mikellides[*] and Darcy L. Allison[†]
Arizona State University, Tempe, AZ 85287, USA

Nalin Ratnayake[‡]
Arizona State University, Tempe, AZ 85287, USA

and

Deborah Booze[§]
Arizona State University, Tempe, AZ 85287, USA

Abstract: The magnetohydrodynamics simulation tool, MACH2 has been upgraded by a thermo-chemical model for ammonia in order to model Pulsed Inductive Thruster, (PIT) operation. This equation of state provides the thermodynamic properties of ammonia, including degree of ionization, for a wide range of pressure and temperature values under thermal non-equilibrium. The thermodynamic functions are utilized in tabular form consistent with the code's established SESAME format. Modeling of the PIT at an energy level of 1764J and propellant mass of 2.1mg confirms capture of the pertinent physical processes and expected trends.

Nomenclature

p	= pressure
T	= temperature
ρ	= mass density
M	= atomic/molecular mass
γ	= ratio of specific heats
e	= specific internal energy
ζ	= average charge (nfe)
θ	= temperature ratio
R	= universal gas constant
C_v	= specific heat at constant volume
V	= voltage
B	= magnetic induction
Eo	= capacitor stored energy
C	= capacitance
Subscripts	
e	= electron
h	= heavy particle
eff	= effective

[*]AST Professor, Department of Mechanical & Aerospace Engineering, Pavlos.Mikellides@asu.edu
[†]Post-Graduate Research Associate, Department of Mechanical & Aerospace Engineering, Darcy.Allison@asu.edu
[‡]Undergraduate Research Assistant, Department of Mechanical & Aerospace Engineering, nalin@asu.edu
[§]Undergraduate Research Assistant, Department of Mechanical & Aerospace Engineering, deborah.booze@asu.edu

I. Introduction

The Pulsed Inductive Thruster (PIT) is a unique propulsion system due to a combination of its distinctive physical operation, demonstrated performance and potential advantages over other electric rockets.[1] A spiral induction coil is powered by a series of capacitors in Marx-loop configurations and produces a strong azimuthal electric field once the pulsed current is passed through. The field breaks down the injected propellant over the surface of the flat coil and the associated radial magnetic field induces an azimuthal current within a thin gas layer. (Fig. 1) This current interacts with the magnetic field to produce an axially-directed electromagnetic force. Such inductive acceleration circumvents the need for electrodes and the erosion-related lifetime limitations that plague traditional electromagnetic thrusters. The PIT could operate with a large range of propellants, however single-shot operation demonstrated optimal performance with polyatomic-molecule fuel. Specifically, the PIT-MkV operating with ammonia at 4.6kJ demonstrated nearly-constant efficiencies exceeding 50% for a wide range of specific-impulse values, Isp; 4000s < Isp < 8000s[1]. Its propensity to work best with such fuels renders the thruster as a potentially ideal candidate for water-propellant operation and associated missions such as In-Situ Propellant Utilization (ISRU) where refueling could be realized by appropriate water-rich cometary rendezvous or by capitalizing on Europa's oceans for deeper space assignments. Its pulsed operation can provide elevated maneuverability – the aforementioned operation produced an impulse range, I, of 0.05N-s < I < 0.12 N-s – which may favor the concept for a number of missions identified by Project Prometheus[2] ranging from direct transfers to desired destinations to on-orbit exploration.

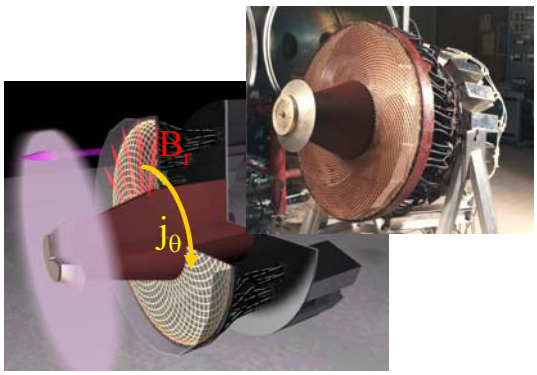

Figure 1. The Pulsed Inductive Thruster (PIT) (Courtesy NGC) and a schematic of the main acceleration process due to the interaction of the applied radial field and the induced azimuthal current.

In order to provide added confidence in the PIT's demonstrated capabilities the magnetohydrodynamics (MHD) code, MACH2 was employed to model its operation and mutually validate by comparisons to experiments.[3] Specifically, the simulations concentrated in modeling PIT operation with helium and argon propellants for a range of propellant mass values and energy levels. The code predicted impulse values that were in excellent agreement with experimental data and provided valuable insights regarding energy deposition to various modes in an attempt to identify dominant energy sinks. The present paper aims to extend the investigation to ammonia propellant by upgrading the numerical tool with the appropriate tabular thermo-chemical model that provides the necessary equation of state. Use of the new thermodynamic model allows simulations of PIT operation with ammonia propellant in order to establish the validity of the model integration and offer preliminary insights to the capabilities of the code in capturing the pertinent physics.

II. Numerical Model

MACH2 is a time-dependent, two-dimensional, axisymmetric, multi-material code that can be applied to problems of complex geometries due to its multi-block structure.[4] The computational mesh can move in an Arbitrary-Lagrangian- Eulerian (ALE) fashion allowing applicability to both diffusive- and dispersive-dominated problems as well as code validation. The mesh can be refined via a variety of adaptive schemes to capture regions of varying characteristic scale. The set of the single-fluid, MHD equations is time-advanced with finite-volume spacial differencing, and the boundary conditions are applied via the ghost-cell technique so that no special conditional statement is necessary at the boundaries.

The mass continuity and momentum equations assume a compressible, viscous fluid with the latter including both real and artificial viscosity effects. The stress tensor can be chosen to evolve under elastic stress for strength of material calculations[5] or modeled as a viscous stress tensor for Newtonian fluid to upgrade the code to a Navier-Stokes solver.[6] The electrons, ions and radiation field are in thermal non-equilibrium, so MACH2 solves up to three energy equations. These include thermal conduction with anisotropic transport and three different models for radiation cooling;

optically-thin Planck radiation, equilibrium and non-equilibrium diffusion radiation.[7] Evolution of the magnetic field is prescribed by the induction equation that includes resistive diffusion, the Hall effect and the thermal source for magnetic fields. Various models for the plasma resistivity are available. They comprise classical anisotropic resistivity,[8] several anomalous resistivity models and contributions from electron-neutral collisions applicable to weakly ionized gases.[9] In many engineering applications the source of magnetic flux is applied currents produced from externally-applied voltage differentials. For this, the code includes a variety of circuit models such as LRC, Pulse-Forming-Networks, sine-waveforms and several others.

The set of the MHD equations is completed by functional relationships for the equations of state, $p_{e,h} = p_{e,h}(\rho, T_{e,h})$, $e_{e,h} = e_{e,h}(\rho, T_{e,h})$, $\zeta = \zeta(\rho, T_e)$, that can be either analytic or tabular. The SESAME library[10] is the tabular model that includes semi-empirical models for the thermodynamic properties, transport coefficients, (including opacities) and average ionization state under local thermodynamic equilibrium. These models have been constructed and are being maintained by the T-1 and T-4 groups at Los Alamos National Laboratory. However, the library did not provide an adequate model for the range of pressure and temperature values that are encompassed by the PIT's propellant gas and in conjunction to similar shortcomings in all thermo-physical literature – ammonia's typical engineering applications, e.g. refrigeration, do not require low density, very high temperature operation – an appropriate ammonia equation of state was developed from basic statistical mechanics principles.

A. The Ammonia Equation of State

The new two-temperature thermo-chemical model[11] computes the thermodynamic properties of ammonia for a range of 100K-232,100K,(20eV), and extends to density values as low as 10^{-7} kg/m^3. The equation of state, (EOS) was computed for all ionized species up to Z=7 charge level for nitrogen, (N) and Z=1 for hydrogen, (H). The dissociation of NH_3 was treated as a complete dissociation into $N_2 + 3H_2$ subsequently followed by the dissociation of molecular nitrogen and hydrogen. The model does not include chemical reactions that produce molecular ions and adhered to the ideal gas and local thermodynamic equilibrium assumptions. An eleven equation, nonlinear system was solved numerically for each data point set, (p, T_h, T_e), and the required thermodynamic properties were recorded for each set in tabular form.

The extended EOS model was validated by comparisons to existing thermo-chemical tables[10] and composition already computed for ammonia. Specifically, the composition was validated with a model developed for use in crystal growth analysis and the thermodynamic properties were validated with the NIST-JANAF tables.[12] Aside from model confirmation the aforementioned comparisons allowed justification of the assumption to exclude alternative ammonia dissociation paths and molecular ionization reactions. However, these existing benchmarks are valid in regions of comparatively low temperature and high pressure as well as for thermal equilibrium between heavy particles and electrons. Thus, validation had to be extended to higher temperature regimes by adjusting the model to compute nitrogen and hydrogen properties individually so as to allow comparisons to an existing model developed by Boulos, et.al.[13] The modifications merely entailed changing the system of equations to individually accommodate N_2 dissociation and the subsequent multiple ionization reactions, and independently address similar chemistry for H_2.

Figure 2 shows the hydrogen composition comparison between Boulos and the code composition output depicted by the solid colored lines. The overall agreement between the two models is very encouraging with slight discrepancies of negligible significance. The discrepancy between the H_2 predictions occurs in a region where the concentration is at least three orders of magnitude less than the maximum and is a consequence of the exclusion of the negatively-charged hydrogen ion. The H composition calculation also displays a slight disagreement; however, the error at 25,000 K is approximately 0.25% between the H variation and the concentration of the dominant H+ and e- species, thus effectively eliminating its overall effect on the plasma mixture.

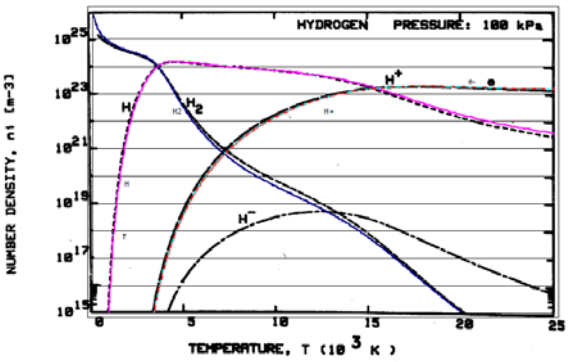

Figure 2. Comparison of hydrogen composition predicted by the code (solid colored) to Boulos' as a function of temperature.

Figure 4 depicts comparisons between the Boulos model and the code output for nitrogen. The overall quantitative agreement between the two models is once again very good with slight discrepancies mostly attributed to the exclusion of certain species by the current effort. Furthermore, most of such discrepancies generally occur when the specie is not a dominant part of the whole gas/plasma mixture's thermodynamic state. Specifically, the discrepancy in the N++ predictions occurs when the specie is two to three orders of magnitude less in concentration and it converges to Boulos' findings at 25,000 K where it begins to reach the higher and more important concentrations. The divergence of the N+ and e- species and N specie are coupled as the N+ specie is higher in concentration than Boulos while the N specie is lower. The N variance is approximately 1% when compared to the concentrations of N+ and e-. The disagreement between the N+ and e- species' concentrations can be attributed to a different choice for the cut-off criterion, a different iteration tolerance, or even slightly different spectroscopic data. However, all aforementioned minor discrepancies between the code and literature composition results do not collectively affect the accuracy of the computed thermodynamic properties as shown in the following section.

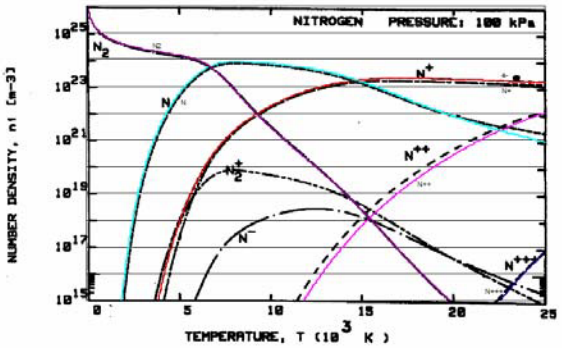

Figure 3. Comparison of nitrogen composition predicted by the code (solid colored) to Boulos' as a function of temperature.

1. Thermodynamic Properties at High Temperatures

Unlike the JANAF tables, the thermodynamic properties calculated by Boulos do include chemical reactions and also include a temperature range where ionization does occur. As mentioned above, reactions associated with N_2 and H_2 are included only. The same modified code that was used to verify composition is again utilized for the thermodynamic property comparisons to the Boulos model. The properties used for the comparisons are the density, i.e. confirmation of the equation of state and the enthalpy, i.e. confirmation of the caloric equation of state. As the ammonia specie was verified using the JANAF tables, all the other species that are present in the ammonia mixture are verified in the Boulos temperature range. In the N_2 case the Boulos temperature range extends high enough to include only the first, second and third N ions to any significant degree. The code system includes these ions and also the higher ions up to the fully-stripped N+7 ion. Verifying the validity of the three lower ions with Boulos also leads to the conclusion that the higher ions' thermodynamic properties can be considered valid. This is because the code subroutines that calculate the thermodynamic properties of the lower ions are the same for the ions not included in Boulos's temperature range. Also, the data used to perform these calculations are all from the same source; Moore's tables.[14]

The following four figures compare the code output and the data from Boulos and display excellent agreement. These confirm the insignificance of the discrepancies identified in the composition comparisons as well as support the assumption to exclude certain chemical reactions that would only increase computational times and perhaps error. There are other points that are noteworthy. The cut-off criterion used to find the correct limits on the sum of the electronic partition function were evidently the same or similar between Boulos and the code system. Calculation of the thermodynamic properties in the higher temperature range can be extremely sensitive to the choice of the cut-off criterion. Also, the species that were neglected from the code system, but were included in the Boulos model do not affect the thermodynamic properties of the mixture. This confirms that the molecular and negative ions were indeed properly neglected from the code mixture.

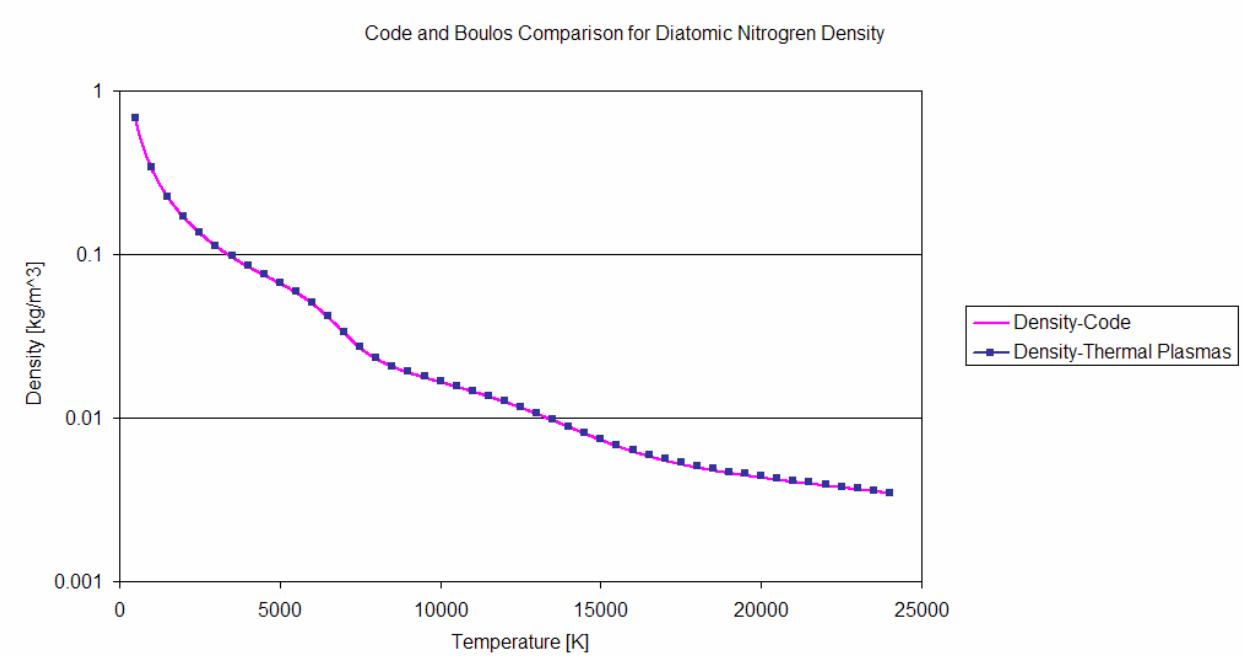

Figure 4. Comparison of the code's computed density profile as a function of temperature, (equation of state) to Boulos' model for nitrogen at 100kPa.

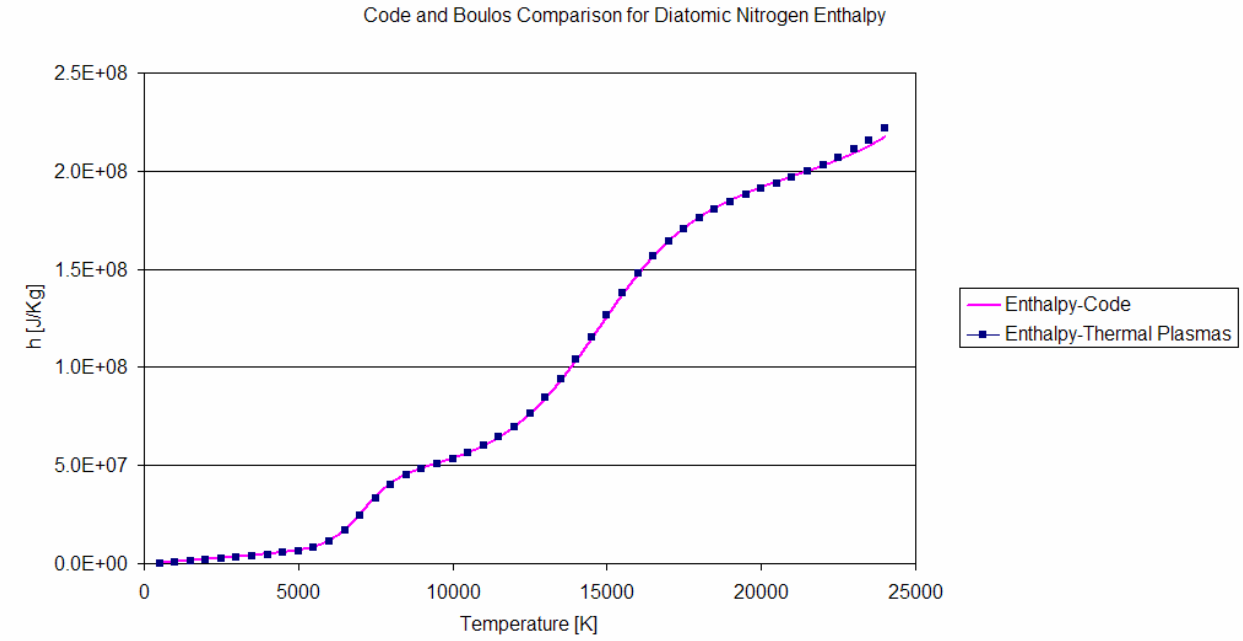

Figure 5. Comparison of the code's computed enthalpy profile as a function of temperature, (caloric equation of state) to Boulos' model for nitrogen at 100kPa.

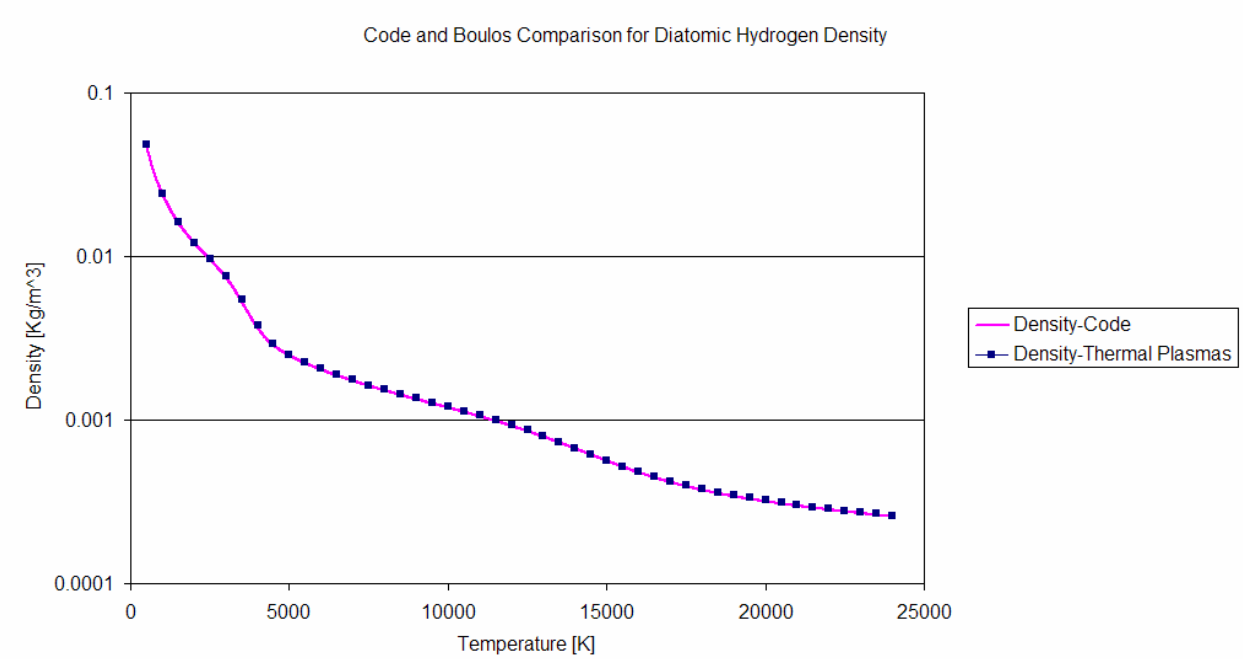

Figure 6. Comparison of the code's computed density profile as a function of temperature, (equation of state) to Boulos' model for hydrogen at 100kPa.

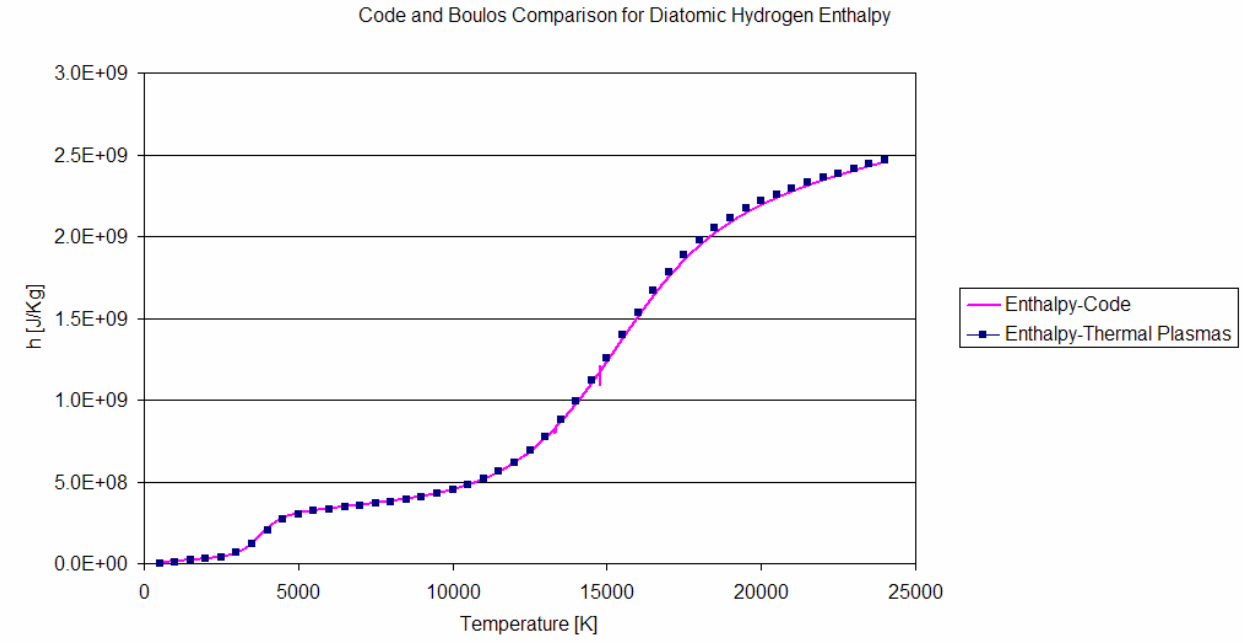

Figure 7. Comparison of the code's computed enthalpy profile as a function of temperature, (caloric equation of state) to Boulos' model for hydrogen at 100kPa.

2. Ammonia EOS for PIT range of operating conditions

Examination of the thermodynamic properties of ammonia in the typical range of temperature and density expected during PIT operation can offer additional insights and options for further model verification. Thus, Fig. 8 and 9 display the behavior of two important thermodynamic properties addressed for this purpose namely the specific internal energy (e) and the number of free electrons per heavy particle (nfe) or average charge, ζ.

The number-of-free-electron-per-heavy-particle profiles do not significantly vary as a function of electron to heavy particle temperature. This is not surprising as nfe is closely coupled to the composition as it is a measure of average charge of the mixture. For example, when the mixture is entirely made up of neutrals then nfe is identically zero. From the last section, it was made clear that the composition in the ionization temperature range is subject to minimal changes for variable θ at constant density. This translates into almost no change in the nfe curves under the same conditions. Several progressive plateaus are identified as the mixture proceeds to sequentially ionize. The most distinctive plateau, as shown in Fig. 8 at a value of nfe=2.0, represents domination of the N+5 ion as the subsequent N ions' formation is delayed due to their substantially higher ionization potentials. It is also noteworthy and expected that the substantial ionization ensues at lower electron temperature values as the mixture's density (or pressure) is decreased. Such distinctive behavior allows for further model confirmation via simple ideal gas calculations.

The specific internal energy follows a fairly predictable curve in all cases and is shown in Fig. 9 again as a

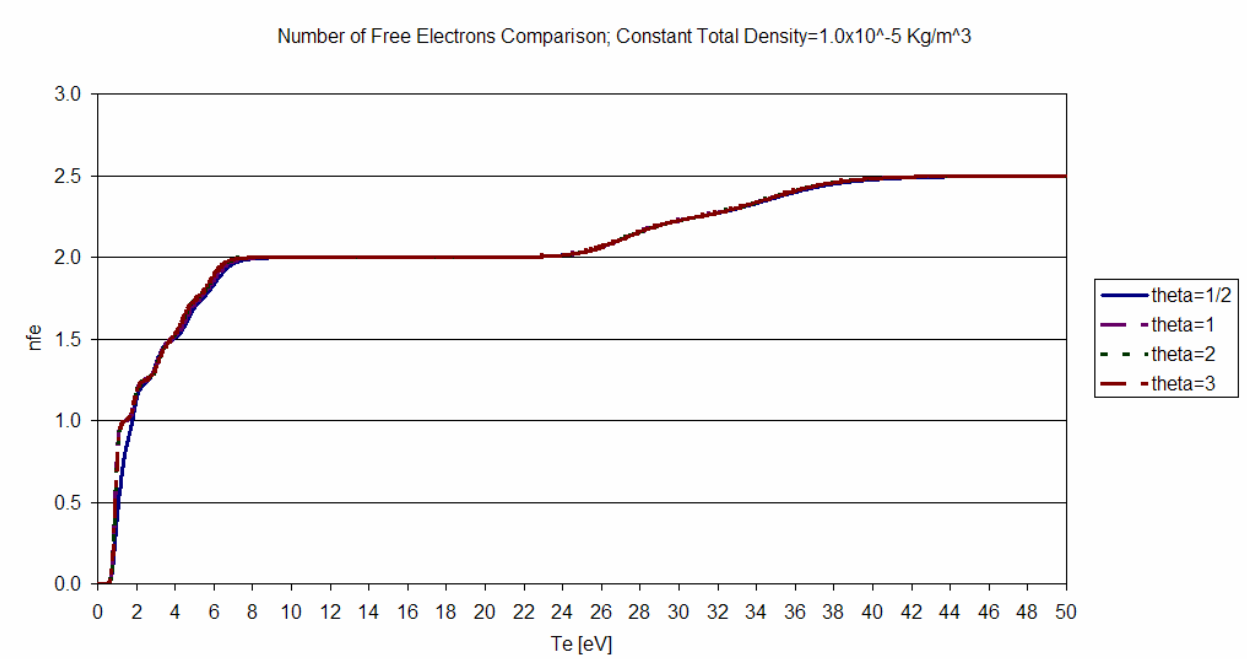

Figure 8. Number of free electrons per heavy particle, (average charge) as a function of electron temperature and varying temperature ratio, $\theta=T_e/T_h$ at $\rho=10^{-5}$ kg/m^3.

function of electron temperature, varying θ, but constant density. Generally, as the mixture stays at a fairly constant composition over some Te range, the specific internal energy variation will be linear. However, over the Te range where reactions occur, such variation is expected to display a steeper positive slope that represents energy deposition to the gas' internal modes as opposed to heating. The successive ionization processes are once again evident by the distinctive steeper positive slopes which of course represent deposition to internal energy modes at approximately constant temperature. The most profound is nitrogen's fifth-level ionization, N+5, which occurs at increasing Te values with increasing density. It is noteworthy, that for a substantial range of electron temperature the mixture consists of only singly-ionized hydrogen and these N+5 ions, (5 eV < Te < 20 eV) without varying substantially with density. This can

be useful for applications that would tend to operate within such a regime and thus could allow approximation of the caloric equation of state as simply $\Delta e = Cv\,\Delta T$, where Cv is the specific heat at constant volume. In addition, this and the N+7 dominated temperature intervals this simplified equation for the internal energy can be used as a further check of

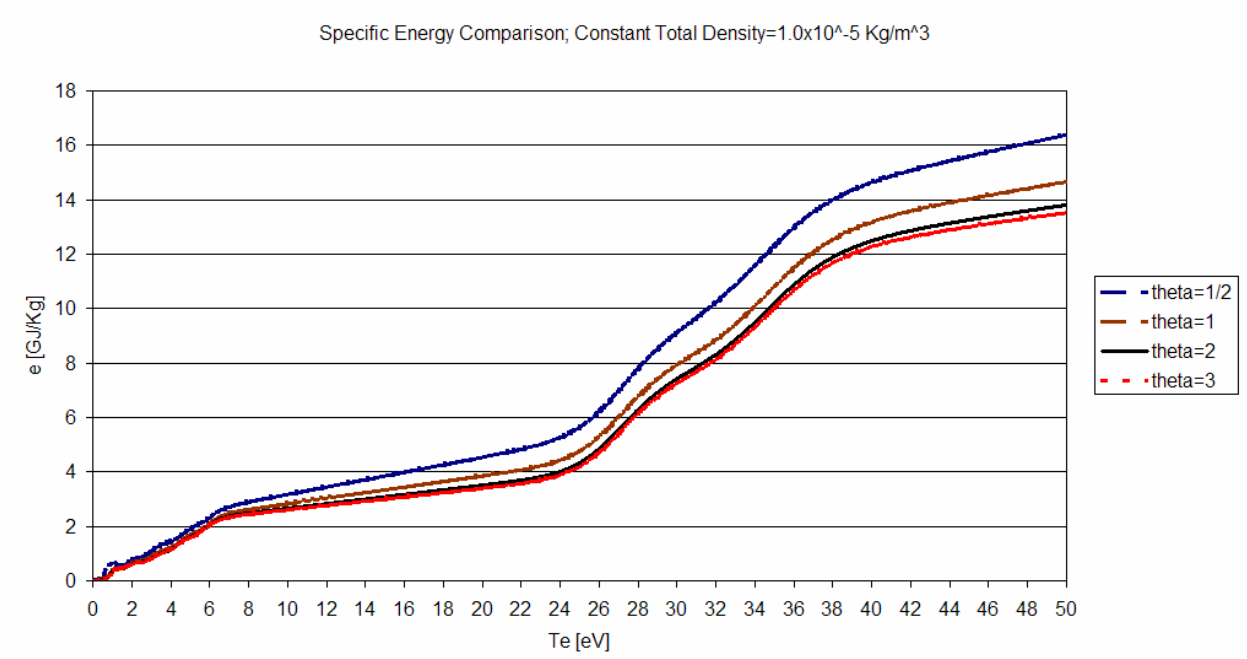

Figure 9. Specific internal energy as a function of electron temperature and varying temperature ratio, $\theta = T_e/T_h$ at $\rho = 10^{-5}$ kg/m^3.

the code output. Specifically, this caloric equation of state is represented by

$$\Delta e = C_v \Delta T = \frac{(\zeta + 1)R}{M(\gamma - 1)} \Delta T \tag{1}$$

where ζ is the average charge or nfe, R is the universal gas constant, M is the average atomic mass of the mixture and γ is the ratio of specific heats. The slope, or C_v, can be calculated where nfe is constant and the mixture is known. Over the range where the mixture is almost entirely made up of only the e-, H+, and N+5 species, the code calculates a C_v value of 8787.8 J/kg-K which is agreement with equation (1). When the mixture is effectively made up of only the e-, H+, and N+7 species, the code calculates a C_v value of 10252.4 which is also confirmed by the simple ideal gas expression. Such comparison serves as further verification as no models were available at this very high temperature range.

III. Pulsed Inductive Thruster Modeling

A. Operating, Initial and Boundary Conditions

A substantial body of experimental data is available for the Pulsed Inductive Thruster (PIT) comprising a diverse range of propellants, energy levels and propellant mass values.1 The power supply consists of a series of 18 capacitors in Marx-loop pairs that are charged in parallel. This results in an effective discharge voltage that is double that of each capacitor's charge voltage which in turn provides the necessary high electric field for breakdown. In particular, the configuration results in an effective capacitance and voltage that relate to the single capacitance and charge voltage through the total energy available:

$$E_o = \frac{1}{2}(\text{number of capacitors}) C V_o^2 = \frac{1}{2} C_{eff} V_{eff}^2 \tag{2}$$

where Vo=1/2Veff. For the polyatomic propellant experiments the effective capacitance was 9μF while the earlier efforts with monatomic propellants utilized smaller capacitors with effective capacitance of 4.5μF. The resulting oscillatory current waveform provided pulse duration of the order of 15μsec with peak currents exceeding 100kA for a range of charge voltage of 10kV < Vo < 16kV and propellant mass of 1.5mg < m < 10mg. Mass is introduced through a nozzle (Fig. 2) by a fast opening gas valve. For optimal distribution of the injected gas the mass-pulse is short enough such that it ceases as the leading edge reaches the confining lexan. The PIT's performance data exhibited approximately constant efficiency trends for a wide range of specific impulse values (500s < Isp < 9000s) providing impulses exceeding 0.1 N-s. Monatomic propellants demonstrated efficiencies on the order of 20% while polyatomic propellants with the higher-capacitance bank dramatically improved exhibiting maximum efficiencies above 50% with ammonia.

The MACH2 simulations utilized the new ammonia equation of state after proper integration by casting the data in the appropriate SESAME tabular form. The physical model included thermal non-equilibrium of a single fluid with classical transport. Boundary conditions modeled thermal and magnetic field insulators with no-slip. The computational grid (Fig. 2) extended well downstream of the thruster's exhaust region to comprehensively capture the acceleration process and assure no influence of the outlet boundary conditions that model variables at zero gradient. Grid resolution was maximized in the vicinity of the coil to assure capture of the fast-rising field's diffusion and associated gradient. In particular, the significant acceleration process occurs during the rise-time, tr~0.9μsec, which implies a characteristic diffusion depth of about 1.78cm for a 2eV plasma, (where m2/s is the electrical diffusivity with Te in eV). The axial grid-cell dimension, z=1.56mm (64 cells in the axial direction) assures accurate capture of the field's gradient with more than 10 cells resolving the diffusion depth.

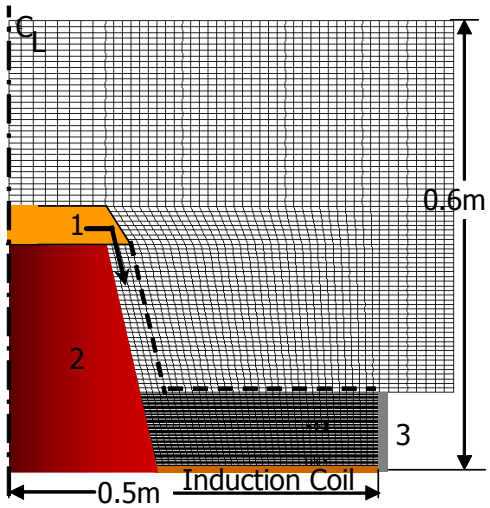

Figure 10.Schematic of the half-plane thruster with the computational grid utilized, (not to scale). 1: Nozzle with pulsed mass-valve, 2: Conical pylon, 3: Confining cuff (lexan).

Initial conditions assigned uniform density in the vicinity of the coil and along the column extending upstream of the injection nozzle (the confined region identified by the dotted line in Figure 2) - to at best resemble the evolved gas injected from the valve - and uniform room temperature, 300K. The significance of non-uniformities present due to the injection scheme have been addressed by a separate series of simulations and showed negligible effects when compared to aforementioned simplified initial conditions. These initial conditions assure that ionization of the gas, which occurs after the breakdown is self-consistently calculated by the MACH2 ionization model along with the evolution of the rest of the pertinent variables as opposed to an assumed initial ionization state. Emulation of the current waveform used the LRC circuit model. Specifically, a circuit model had been developed[2] to calculate the PIT's current waveform with significant accuracy. For the MACH2 simulation the LRC external parameters were adjusted to as-best match the important features of the aforementioned model with the typical current waveform shown in Fig. 11.

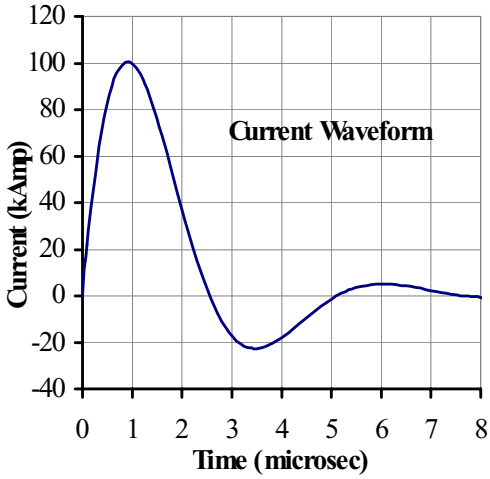

Figure 11. MACH2 calculated Current Waveform used to emulate the PIT's circuitry, Veff = 28kV.

B. Modeling Results

The objective of the simulation included in this paper is to establish the proper integration of the new ammonia model into the

MACH2 code and qualitatively capture expected behavior of the pertinent variables as a function of time and two dimensions.

The following series of Figures aim to capture the behavior of the accelerating plasma for a total capacitor stored energy, Eo=1764J (emulated at an effective capacitance of 4.5μF) and 2.1mg of propellant mass. Figure 12 depicts the time dependence of the radial magnetic field at a radial location of 40cm and two axial, downstream locations of 0.5cm and 5cm. The expected field diffusion is evident by the decreasing magnetic field peak values in addition to convection by the increasing time value at which the peaks occur. One of the more interesting features however, is that MACH2 predicts a substantial gradient of the magnetic field when one compares the peak value at 0.5cm, B_r~0.23T to the maximum value of the field calculated by assuming uniform radial magnetic, i.e. $B_{rmax} = \mu_o J/(r_o - r_i) = 0.418$T. This implies that the coupling of plasma and magnetic flux at this energy and mass level occurs over a wider portion which in turn suggests diminished induced azimuthal currents. The simulation invokes a classical resistivity model which does include electron-neutral collisions[2], but does not account for anomalous transport that may be expected within the lower density regions upstream of the bulk of the accelerating gas.

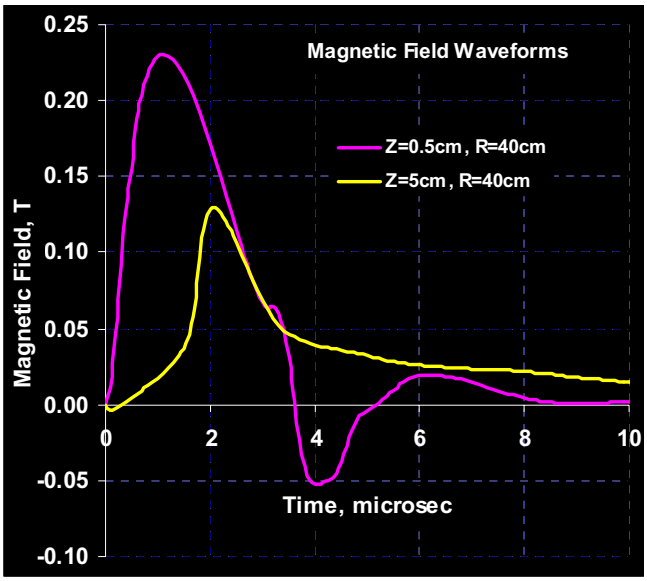

Figure 12. Radial Magnetic Field waveforms computed by MACH2 at a radial location of 40cm and axial locations of 0.5cm and 5cm. Eo=1764J, m=2.1mg.

The two-dimensional distributions of constant magnetic field lines, shown in Figs. 13-15 for three different times early during the discharge, depict the approximately uniform distribution of the predominantly radial magnetic field which implies that the magnetic field waveforms depicted in Fig. 12 are representative of the behavior of the field for any radial location. This is expected and has been implied by analysis of the experimental data[1] which lends added confidence to the code's ability to capture the physical processes.

Figures 16 and 17 aim to describe the plasma advancement after the effective pulse duration, i.e. at approximately 10 μsec, and serve as further confirmation of the proper integration of the ammonia equation of state to the MACH2 code. The mass density profile depicts the expected trend of the bulk of the plasma – identified by the elevated values encompassed within 6-8cm – being entrained by the upstream propellant which is still under the partial influence of the Lorentz force. We note from the average charge profile that downstream of the 6cm location the plasma is not fully ionized which confirms the expected snowplow effect. Closer to the coil the plasma's density is about one order of magnitude less than the maximum value occurring at about 6cm which further quantifies the degree of plasma and magnetic flux coupling. The pressure profile supports the same interpretation regarding the plasma dynamics, but it also serves as further confirmation of the ammonia thermodynamic model. Specifically, at z=6cm, the average charge, ζ=0.995, electron temperature, Te=1.43eV, the mass density, ρ=1.14e-5kg/m^3 and the plasma pressure is calculated at p=739Pa. This is in accordance to $p=(1+\zeta)\rho RT$ assuming thermal equilibrium which is the case for this regime of operation.

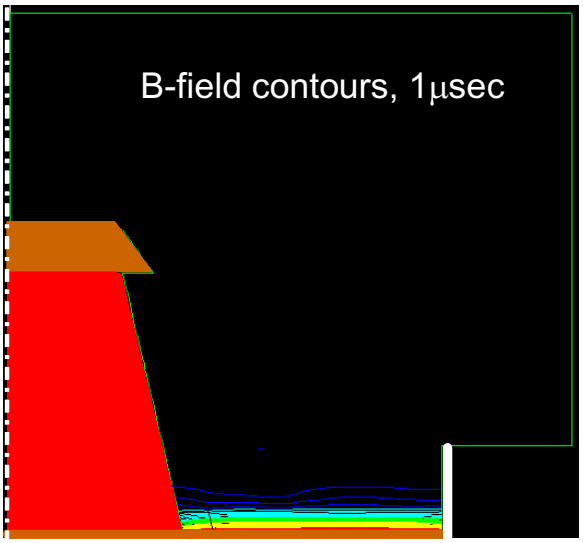

Figure 13. Magnetic Field contours for NH_3 at 1 μsec. Eo=1764J, m=2.1mg.

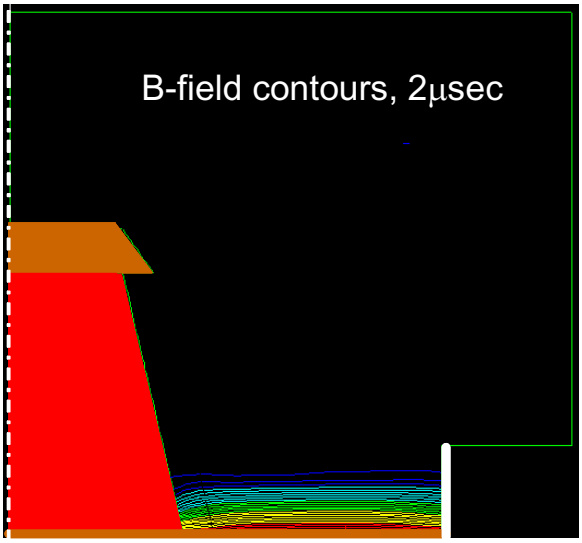

Figure 14. Magnetic Field contours for NH_3 at 2 μsec. Eo=1764J, m=2.1mg.

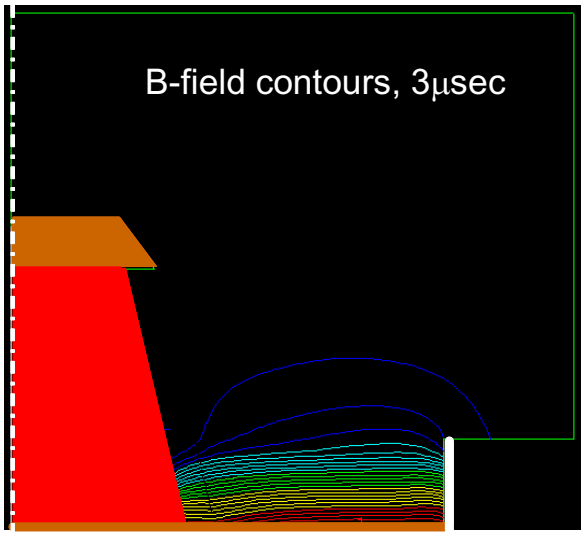

Figure 15. Magnetic Field contours for NH_3 at 3 μsec. Eo=1764J, m=2.1mg.

IV. Conclusions

The magnetohydrodynamic, (MHD) code, MACH2 has been upgraded with a two-temperature NH_3 thermo-chemical model to allow simulations of the Pulsed Inductive Thruster, (PIT) operating with ammonia propellant. The model's computed composition and thermodynamic properties have been verified in multiple ways including high temperature comparisons to similar models. The equations of state have been cast in the proper tabular form to allow integration to the MACH2 code. Preliminary modeling of PIT operation at a single energy level and ammonia propellant mass value have depicted expected trends and allow initial characterization of the plasma under such inductive acceleration scheme. Furthermore, the affirmatory outcome allows for advancement of the modeling to a diverse range of energy levels and propellant mass values and eventual comparisons to experimental data.

V. Acknowledgments

The authors acknowledge Mr. Eric Pencil's helpful comments. The work was supported by NASA under Project Prometheus; the Nuclear-electric Pulsed Inductive Thruster (NuPIT) System. (MSFC Task Agreement Number: AT-05-06 NASA GRC Contract Management Number: NNC04GB66G)

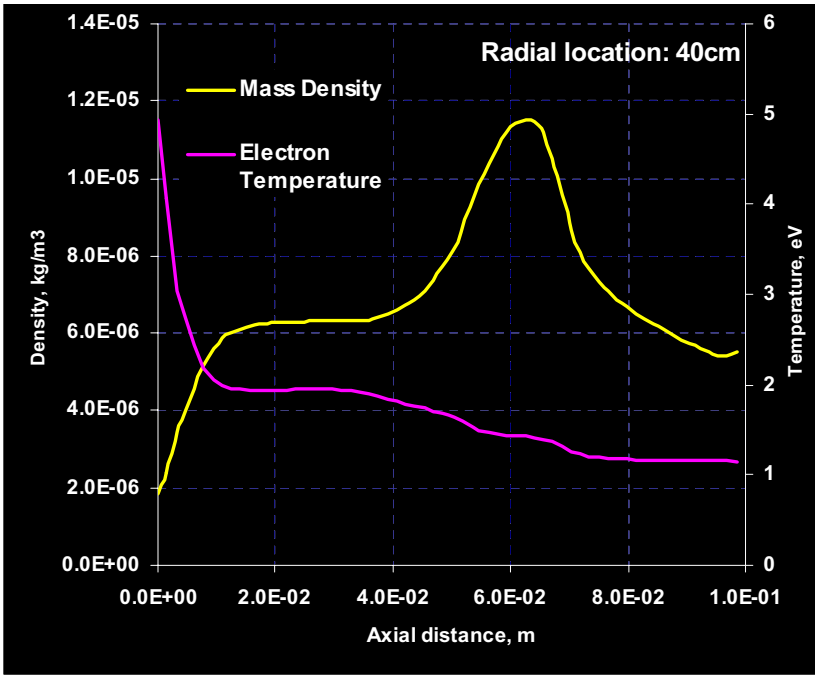

Figure 16. Mass Density and Electron Temperature profiles as a function of axial distance, z at 10μsec. Eo=1764J, m=2.1mg.

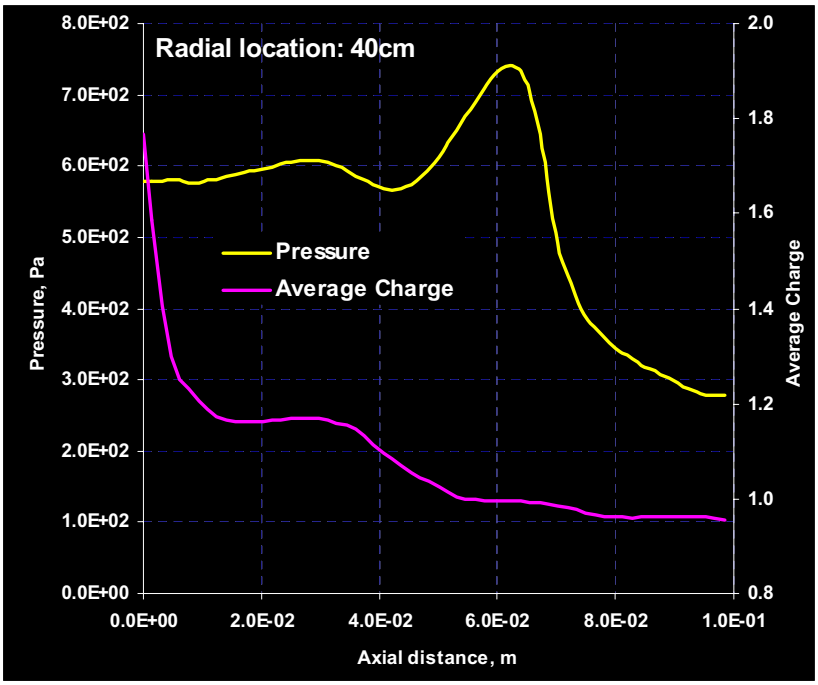

Figure 17. Plasma Pressure and Average degree of Ionization profiles as a function of axial distance, z at 10μsec. Eo=1764J, m=2.1mg.

VI. References

1. Dailey, L.C. and Lovberg, R.H., "The PIT MkV Pulsed Inductive Thruster," NASA Contractor Report 191155, July 1993.

2. http://www.hq.nasa.gov/office/oss/missions/prometheus.htm

3. Pavlos G. Mikellides and Chris Neilly, "Pulsed Inductive Thruster, Part 1: Modeling, Validation and Performance Analysis," AIAA-2004-4091, 40th AIAA/ASME/SAE/ASEE Joint Propulsion Conference and Exhibit Fort Lauderdale, FL, July, 2004.

4. Frese, M.H., "MACH2: A Two-Dimensional Magnetohydrodynamics Simulation Code for Complex Experimental Configurations," AMRC-R-874, September 1986.

5. Peterkin, R.E., Jr., and Frese, M.H., "A Material Strength Capability for MACH2," MRC/ABQ-R-1191, October 1989.

6. Mikellides, P.G., "A Theoretical Investigation of Magnetoplasmadynamic Thrusters," Ph.D. Dissertation, Department of Aeronautical and Astronautical Engineering, The Ohio State University, 1994.

7. Douglas, M.R., "Radiation Production from Stagnating Compact Toroids Employing a Nonequilibrium Radiation Diffusion Model," Ph.D. Dissertation, U. of New Mexico, 1994.

8. Braginskii, S.I., "Transport Processes in a Plasma," in Review of Plasma Physics, M.A. Leontovich, ed. Consultants Bureau, New York, 1965.

9. Degnan, J.H., Peterkin, R.E., Jr. et. al., "Compact Toroid Formation, Compression, and Acceleration," Physics of Fluids, B5 (8), 2938, 1993.

10. Holian, K.S., ed, "T-4 Handbook of Material Properties Data Base.. Vol Ic: EOS," LA-1160-MS, Los Alamos National Laboratory, Los Alamos, NM, November, 1984.

11. Darcy L. Allison and Pavlos G. Mikellides, "Pulsed Inductive Thruster, Part 2: Two-Temperature Thermochemical Model for Ammonia," AIAA-2004-4092, 40th AIAA/ASME/SAE/ASEE Joint Propulsion Conference and Exhibit Fort Lauderdale, FL, July, 2004.

12. Chase, Malcolm W. Jr., *Journal of Physical and Chemical Reference Data: NIST-JANAF Thermochemical Tables.* ed. 4th Monograph No. 9 Parts 1 & 2 (American Institute of Physics and the American Chemical Society, Woodbury NY, 1998).

13. Maher I. Boulos, Pierre Fauchais, and Emil Pfender, *Thermal Plasmas* (Plenum Press, New York, 1994), pp. 255, 258-259.

14. Charlotte E. Moore, *Tables of Spectra of Hydrogen, Carbon, Nitrogen, and Oxygen Atoms and Ions*, edited by Jean W. Gallagher (CRC Press, Boca Raton, 1993).